International Journal of Heat and Mass Transfer 121 (2018) 153–169

Contents lists available at ScienceDirect

International Journal of Heat and Mass Transfer

journal homepage: www.elsevier.com/locate/ijhmt

An experimental, computational and flow visualization study on the air-side thermal and hydraulic performance of louvered fin and round tube heat exchangers

Abdulkerim Okbaz [a,*], Ali Pınarbaşı [a], Ali Bahadır Olcay [b], Muharrem Hilmi Aksoy [c]

[a] Yildiz Technical University, Faculty of Mechanical Engineering, Besiktas, Istanbul 34349, Turkey
[b] Yeditepe University, Mechanical Engineering Department, Atasehir, Istanbul 34755, Turkey
[c] Selcuk University, Mechanical Engineering Department, Selcuklu, Konya 42075, Turkey

ARTICLE INFO

Article history:
Received 22 June 2017
Received in revised form 10 December 2017
Accepted 23 December 2017

Keywords:
CFD
Colburn factor *j*
Compact heat exchanger
Fanning friction factor *f*
Flow visualization
Heat exchanger
Heat transfer
Heat transfer enhancement
Louvered fin
PIV
Pressure drop
Wavy fin

ABSTRACT

The aim of this study is to determine heat transfer and pressure drop characteristics in different louvered fin geometries for manufacturing of commercial louvered fin and round tube heat exchangers. Numerical simulations were carried out for various louver angles, louver lengths (pitches), fin pitches and frontal air velocities. The heat transfer and pressure drop characteristics of the louvered fin and round tube heat exchangers, Colburn and friction factors, were respectively normalized with Colburn and friction factors of the flat plate fin and round tube heat exchangers operating under the same conditions and they were presented as the relative Colburn factor j^* and the relative friction factor f^*. Thermal & hydraulic performance was presented as JF^*. Temperature and local Nusselt number contours, and streamline patterns were provided to reveal the mechanisms behind the heat transfer enhancement. Among different heat exchangers for which heat transfer and pressure drop characteristics were obtained, one was chosen to manufacture a real size heat exchanger. Flow visualization studies were also conducted with a PIV system in an open water channel to determine whether the flow structure is louvered directed or not. The louvered fin heat exchanger tested in the PIV system was a five times scaled up model of the real size louvered fin heat exchanger and made from a transparent plexiglas material. PIV results were presented and evaluated based on streamlines and velocity vectors. Furthermore, a numerical analysis was performed using exactly the same dimensions and conditions of the model tested in the PIV system. The comparison between numerical and experimental results was done to validate the numerical model. Consequently, the performance of the fabricated real size heat exchanger was tested at different air velocities in a wind tunnel in a conditioned room. The experimental results were compared with numerical analyses and found to be compatible with each other. Finally, thermal and hydraulic performance of the louvered fin and round tube heat exchanger was compared with a wavy fin and round tube heat exchanger with identical size and specifications. It was found that the thermal and hydraulic performance of the louvered fin and round tube heat exchanger is higher than that of the wavy fin and round tube heat exchanger. The Colburn factor *j*, friction factor *f* and *JF* of the louvered fin and round tube heat exchanger are higher about 16.8–7%, 19.9–8.2% and 10–4.3% than that of the wavy fin and round tube heat exchanger depending on the Reynolds number, respectively.

© 2017 Elsevier Ltd. All rights reserved.

1. Introduction

Heat exchangers are used in a wide range of industrial and everyday applications from air and sea to land vehicles, from power plants to air conditioning. Increasing the thermal and hydraulic performance of heat exchangers means saving energy and materials at a considerable amount. For this reason, researchers at universities and manufacturers have been conducting studies to increase the performance of heat exchangers for years. Louvered fins are a cost-effective method for increasing the thermal and hydraulic performance of heat exchangers. The louvered fins, which provide non-continuous interrupted surfaces, increase the air-side heat transfer coefficient in two ways. First, the discontinuous solid wall in contact with the fluid flow reduces thickness of the thermal boundary layer by stopping its growth. Second, air

* Corresponding author.
E-mail address: aokbaz@yildiz.edu.tr (A. Okbaz).

https://doi.org/10.1016/j.ijheatmasstransfer.2017.12.127
0017-9310/© 2017 Elsevier Ltd. All rights reserved.

Nomenclature

A	area (m^2)
A_c	inlet frontal flow area (m^2)
A_f	fin surface area (m^2)
A_o	total outside surface area (m^2)
A_i	tube inside surface area (m^2)
$c_{p,c}$	specific heat of cold fluid (J/kg °C)
$c_{p,h}$	specific heat of hot fluid (J/kg °C)
d_i	inside tube diameter (m)
d_o	outside tube diameter (m)
f	the Fanning friction factor
f^*	the relative Fanning friction factor
F_L	flow length (m)
H	fin pitch (m)
h	heat transfer coefficient (W/m^2 °C)
h_o	air side heat transfer coefficient (W/m^2 °C)
h_w	water level in open water channel (mm)
j	the Colburn factor
j^*	the relative Colburn factor
k	turbulent kinetic energy
L_p	louver pitch (m)
L_T	tube length (m)
Nu	Nusselt number
U	overall heat transfer coefficient (W/m^2 °C)
P_l	longitudinal tube pitch (m)
P_r	Prandtl number
P_t	transverse tube pitch (m)
r	radius of tube diameter, with collar fin thickness (m)
Re	Reynolds number
Re_H	Reynolds number based on fin pitch
Re_{L_p}	Reynolds number based on louver pitch
Re_{d_o}	Reynolds number based on outside tube diameter
R_{eq}	equivalent radius for circular fin (m)
St	Stanton number
T	temperature (°C)
ΔT_m	logarithmic mean temperature difference (°C)
$T_{c,in}$	inlet temperature of cold fluid (°C)
$T_{c,out}$	outlet temperature of cold fluid (°C)
$\dot{m}_c$	cold fluid mass flow rate (kg/s)
$\dot{m}_h$	hot fluid mass flow rate (kg/s)
$T_{h,in}$	inlet temperature of hot fluid (°C)
$T_{h,out}$	outlet temperature of hot fluid (°C)
T_w	wall temperature (°C)
$U_{frontal}$	frontal air velocity (m/s)
X_L	geometric parameter (m)
X_M	geometric parameter (m)
W_λ	wave length of wavy fin (m)
W_h	wave height of wavy fin
ΔP	pressure drop (Pa)
$\dot{Q}_h$	hot fluid heat transfer rate (W)
$\dot{Q}_c$	cold fluid heat transfer rate (W)
$\dot{Q}$	averaged heat transfer rate (W)

Greek symbols

μ	dynamic viscosity (kg/m s)
δ_f	fin thickness (m)
η_f	fin efficiency
η_o	surface efficiency
θ	louver angle (°)
λ	thermal conductivity (W/m °C)
ρ	density of fluids (kg/m^3)
υ	kinematic viscosity (m^2/s)

Subscript

a	air
c	cold fluid
h	hot fluid
i	inside
in	inlet
k	turbulent kinetic energy
o	outside
out	outlet
ref	reference
t	tube
f	fin

circulates between the different fins by increasing the mixture of cold and hot fluids due to the effect of the louvers. It is necessary that the air follows the louvers yielding heat transfer enhancement. This kind of flow is called louver-directed flow, which is dependent on the Reynolds number and geometric parameters. On the other hand, louvered fins increase the pressure drop as they allow the flow to circulate between fins increasing the flow length. For this reason, the maximum possible heat transfer enhancement should be achieved with the lowest pressure drop possible. Some of the studies in the literature related to louvered fin heat exchangers are grouped as experimental, numerical and correlation studies and summarized below.

Experimental studies about louvered fin heat exchangers can generally be divided into two groups. Studies investigating in detail the effect of flow structure on heat transfer and pressure drop may be included into the first group. In such studies, scaled models of real size heat exchangers were investigated. To conduct this kind of experimental studies, Springer and Thole [1] developed a methodology to design an experimental model which was scaled up by a factor of 20 for two-dimensional louvered fin geometries. They concluded that a total number of 19 louvered fin rows must be used to simulate a full-scale louvered fin heat exchanger. Lyman et al. [2] proposed a method to determine heat transfer coefficients of louvered fin heat exchangers. They performed experiments using large-scale louvered fin models with different fin pitches and louver angles and determined convective heat transfer coefficients using the bulk flow temperature and adiabatic wall temperature as reference temperatures. DeJong and Jacobi [3] conducted a complementary flow visualization study and naphthalene sublimation technique to investigate the relation between flow structure and heat transfer characteristics on louvered fins in the effect of bounding walls. T'Joen et al. [4] and Huisseune et al. [5] used a dye injection technique to visualize the flow structure around louvered fins.

In the other group, experiments were conducted using full-scale commercially available heat exchangers. In such studies, the total effects of fluid properties, operating conditions and geometrical parameters on heat transfer and pressure drops were investigated.

Wang et al. [6] developed a correlation for heat, momentum and mass transfer with mean deviations of 5.94%, 6.10%, and 7.89% based on their experimental data, respectively. Kim and Bullard [7] concluded that flow depth is a dominant parameter on pressure drop, and that the effect of louver angle on heat transfer rate depends on the flow depth, fin spacing and Reynolds number. Qi et al. [8] reported that there are three main geometrical factors, such as ratio of fin pitch, fin thickness and the number of louvers

to design an optimal heat exchanger. Vaisi et al. [9] found that heat transfer was increased by 9.3% and pressure drop was decreased by 18.20% for a symmetrical arrangement compared to an asymmetrical arrangement of louvered fins. In their experimental study Dogan et al. [10] found that using double-row fins is more effective than that of triple-row in terms of the Number of Transfer Units (NTU). Shojaeefard and Zare [11] developed a one dimensional finite element method to determine condenser performance and used their method for the optimization of louvered-fin heat exchangers. Torregrosa-Jaime et al. [12] developed a semi-empirical correlation to determine the heating and cooling capacity of the tested compact louvered-fin and flat-tube heat exchangers.

In addition to experimental studies, there is a growing number of Computational Fluid Dynamics (CFD) studies investigating the thermal and hydraulic performance of louvered fin heat exchangers due to increasing computing power and recent progress in CFD software. Atkinson et al. [13] and Perrotin and Clodic [14] numerically investigated heat transfer and pressure drop characteristics using 2D and 3D models of 1-row automotive air conditioning condensers for different frontal air velocities. Both reported that 3D models which predict heat transfer characteristics are in a better agreement with experimental measurements than 2D models. Leu et al. [15] numerically studied heat transfer and pressure drop characteristics of louvered fin heat exchangers with circular and oval tubes for different louver angle, louver pitch and louver lengths. Jang et al. [16] suggested a method to find an optimum louver angle for louvered fin heat exchangers. Malapure et al. [17] concluded that air moves in the direction of fins at low Reynolds numbers while its flow follows louvers at high Reynolds numbers. Hsieh and Jang [18] reported that fin collar outside diameter, transverse tube pitch and fin pitch are the dominant parameters which affect the thermal and hydraulic performance of the heat exchanger. Mao et al. [19] developed a model based on the finite element method to describe thermal and hydraulic characteristics of multi-louvered fin and flat tube heat exchangers under flow maldistribution. Ferrero et al. [20] investigated the influence of fin pitch, louver length and louver angle on heat transfer and pressure drop characteristics of louvered fin heat exchanges. They concluded that there is not one optimum configuration for heat exchangers. They suggested a procedure that considers industrial constrains to optimize louvered fin heat exchangers. Ameel et al. [21] explained how to correctly evaluate the performance of various heat exchangers for accurate corresponding Reynolds numbers. Karthik et al. [22] studied the effect of various geometrical parameters such as fin pitch, transverse tube pitch, longitudinal tube pitch, louver pitch and louver angle on thermal and hydraulic performance of louvered fin heat exchangers. Sangtarash and Shokuhmand [23] experimentally and numerically studied the effect of dimples with different configurations on heat transfer and pressure drop characteristics of louvered fin heat exchangers. Jang and Chen [24] used the conjugate gradient method to numerically investigate the thermal and hydraulic performance of a louvered fin heat exchanger with a variable louver angle. In another study, Liang et al. [25] performed numerical and experimental studies and they concluded that heat transfer capacity increased when louvered fins with 5.4 mm height were used instead of louvered fins with 8 mm height for a condenser in the same size. Okbaz et al. [26] and Okbaz et al. [27] numerically investigated thermal and hydraulic performance of louvered fin and round tube heat exchangers. Okbaz et al. [28] numerically studied the influence of louver angle on heat transfer and pressure drop of louvered fin heat exchangers. They also conducted flow visualization experiments to investigate the relation between thermal and hydraulic performance and flow efficiency.

Using various experimental results, Wang et al. [29], Dong et al. [30] and Ryu and Lee [31] obtained some correlations to determine heat transfer and pressure drop characteristics of louvered fin heat exchangers.

The studies in the literature show that the thermal and hydraulic performance of heat exchangers varies strongly with fin forms. Many correlations have been developed to predict the air-side heat transfer coefficient. However, these correlations can produce large differences for the air side heat transfer coefficient. This variation creates difficulties in the design of heat exchangers to be used for specific purposes since correlations cannot be used very effectively to improve heat transfer characteristics of a given product. The aim of this study is to design louvered-fins for heating and cooling heat exchanger and condensers in the manufacturing list of FRITERM Inc. in Turkey. For this purpose, heat transfer and pressure drop characteristics for different fin pitches, louver angles, and louver lengths at different air velocities were determined using the CFD approach and experimental measurements were conducted in a wind tunnel and by particle image velocimetry (PIV) method in a water channel. The thermal and hydraulic performance of the louvered fin and round tube heat exchanger was compared with that of a wavy fin and round tube heat exchanger with identical size and specifications. As a result, the thermal and hydraulic performance of the louvered fin and round tube heat exchanger was higher than that of the wavy fin and round tube heat exchanger.

2. Numerical method

2.1. Governing equations

Governing differential equations for the velocity and temperature fields were solved using commercial software ANSYS Fluent 16.2 based on a control volume method. The fluid was considered as an ideal gas with constant properties based on averaged temperature values and the fluid flow was assumed to be three dimensional, incompressible and turbulent. Several turbulence models including standard k-ε turbulence, RNG k-ε turbulence, realizable k-ε turbulence, and Reynolds stress model (RSM) were tested. In addition to turbulence, separation effects in the vicinity of the tubes were considered when solving the three dimensional flow fields. Furthermore, PIV measurements were performed at Selcuk University (Konya, Turkey) and wind tunnel tests were conducted at the Friterm Inc. R&D laboratory (Istanbul, Turkey) to validate the numerical model with experimental findings. Specifically, when the heat transfer results of the numerical and experimental studies were compared, it was observed that RNG k-ε turbulence model, realizable k-ε turbulence model and the Reynolds stess model predicted convective heat transfer coefficient closer to the experimental results than those of the standard k-ε model. However, more CPU time and memory were required for the Reynolds stess model simulations. Besides, Hsieh and Jang [18] recommend the extended k-ε turbulence model. Since the realizable model provides the best performance of all the k-ε turbulence models of separated flows [32], this model was decided to be used for calculations of the three-dimensional flow and temperature fields because of its low cost running time and established good performance on simulating heat transfer problems of this kind. Enhanced wall treatment was utilized to resolve the viscous sublayer and fully turbulent region [32].

The governing equations representing the conservation of mass, momentum and energy are as follows:

$$\frac{\partial}{\partial x_i}(\rho u_i) = 0 \tag{1}$$

$$\frac{\partial}{\partial x_i}(\rho u_i u_j - \tau_{ij}) = \frac{\partial p}{\partial x_j} + S_{ij} \tag{2}$$

where τ_{ij} is the viscous stress tensor:

$$\tau_{ij} = 2\mu S_{ij} - \frac{2}{3}\mu \frac{\partial u_k}{\partial x_k}\delta_{ij} \tag{3}$$

$$S_{ij} = \frac{1}{2}\left(\frac{\partial u_i}{\partial x_j} + \frac{\partial u_j}{\partial x_i}\right) \tag{4}$$

$$\frac{\partial}{\partial x_i}\left(\rho u_i h - \lambda \frac{\partial T}{\partial x_i}\right) = u_i \frac{\partial p}{\partial x_i} + \tau_{ij}\frac{\partial u_i}{\partial x_i} \tag{5}$$

The transport equations for k and ε are for the realizable k-ε model:

$$\frac{\partial}{\partial x_i}(\rho k u_i) = \frac{\partial}{\partial x_j}\left[\left(\mu + \frac{\mu_t}{\sigma_k}\right)\frac{\partial k}{\partial x_j}\right] + G_k - \rho\varepsilon - Y_M + S_k \tag{6}$$

$$\frac{\partial}{\partial x_i}(\rho \varepsilon u_i) = \frac{\partial}{\partial x_j}\left[\left(\mu + \frac{\mu_t}{\sigma_\varepsilon}\right)\frac{\partial \varepsilon}{\partial x_j}\right] + \rho C_1 S_\varepsilon - \rho C_2 \frac{\varepsilon^2}{k + \sqrt{v\varepsilon}} + S_\varepsilon \tag{7}$$

$$C_1 = \max\left[0.43, \frac{\eta}{\eta + 5}\right], \eta = S\frac{k}{\varepsilon} \text{ and } S = \sqrt{2S_{ij}S_{ij}} \tag{8}$$

Here, G_k represents the generation of turbulence kinetic energy due to the mean velocity gradients. Y_m represents the contribution of the fluctuating dilatation in compressible turbulence to the overall dissipation rate. C_2 is constant. σ_k and σ_ε are the turbulent Prandtl numbers for k and ε, respectively while S_k and S_ε are user-defined source terms [32]. The eddy viscosity is computed by

$$\mu_t = \rho C_\mu \frac{k^2}{\varepsilon} \tag{9}$$

where

$$C_\mu = \frac{1}{A_0 + A_s \frac{kU_*}{\varepsilon}} \tag{10}$$

$$U^* \equiv \sqrt{S_{ij}S_{ij} + \widetilde{\Omega_{ij}}\Omega_{ij}} \tag{11}$$

$$\widetilde{\Omega_{ij}} = \Omega_{ij} - 2\varepsilon_{ijk}\omega_k \text{ and } \Omega_{ij} = \overline{\Omega_{ij}} - \varepsilon_{ijk}\omega_k \tag{12}$$

The model constants are $A_0 = 4.04$ and $A_s = \sqrt{6}\cos\phi$ where

$$\phi = \frac{1}{3}\cos^{-1}(\sqrt{6}W), W = \frac{S_{ij}S_{jk}S_{ki}}{\widetilde{S}^3}, \widetilde{S} = \sqrt{S_{ij}S_{ij}}, S_{ij} = \frac{1}{2}\left(\frac{\partial u_j}{\partial x_i} + \frac{\partial u_i}{\partial x_j}\right) \tag{13}$$

2.2. Details of computational fluid dynamics model

The pressure based coupled algorithm was employed as a velocity–pressure coupling algorithm because of its superiority for solution convergence. A second-order upwind scheme was utilized for spatial discretization of the governing equations while the least-squares cell-based gradient evaluation method was used to compute the gradient of the scalar values, secondary diffusion terms and velocity derivatives. A second-order pressure interpolation scheme was employed to interpolate the pressure values at the faces. The iterations continued until the residuals of continuity, momentum, turbulence kinetic energy and turbulence dissipation rate equations were lower than 10^{-5} and that of energy remained below 10^{-9}.

The computational domain and mesh structure are illustrated in Fig. 1. The quality of the mesh was carefully assessed during the mesh generation process based on average skewness value of

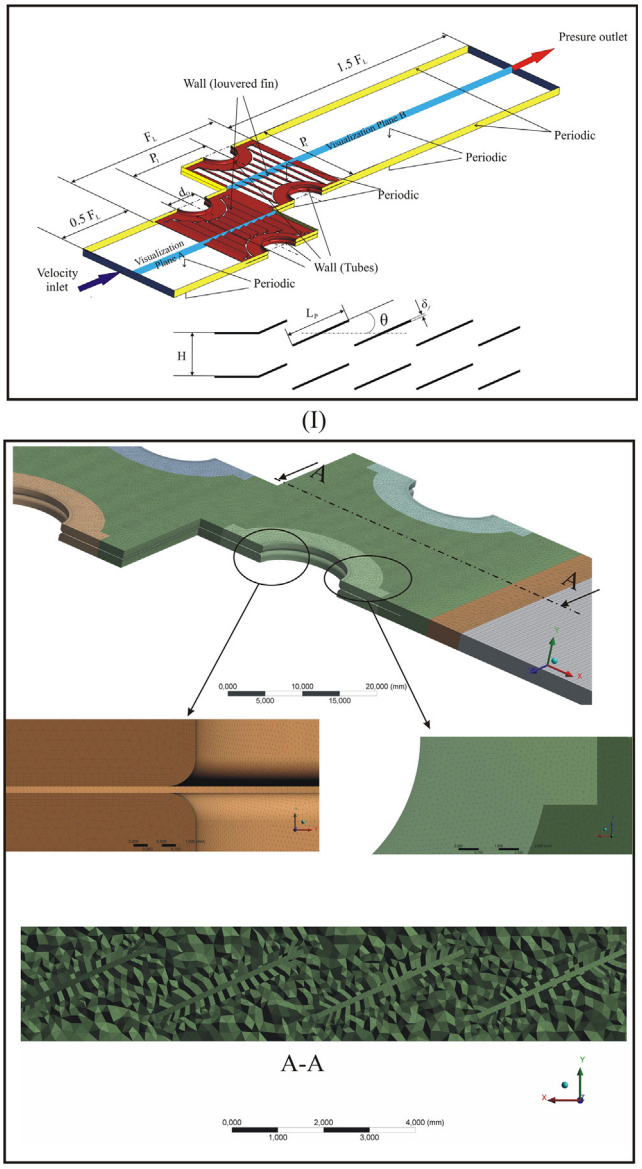


Fig. 1. 3D computational domain and boundary conditions (I); Computational grid system (II).

0.20 and maximum skewness value of 0.60. A multi-block hybrid method was applied dividing the computational domain into several subdomains to provide better quality and sensitivity of the mesh structure. More specifically, meshes with five layers of prism elements were established in the region close to the fin and tube walls while unstructured tetrahedron meshes were used in the outer region. A structured hexahedral mesh was employed in the extended inlet and outlet regions.

The dimensions of extended upstream and downstream regions were chosen as $0.5F_L$ and $1.5F_L$, respectively as shown in Fig. 1 to ensure a uniform velocity profile at the inlet and fully developed flow condition at the outlet. Here, F_L is flow length and boundary conditions of the computational domain were chosen based on the heat exchanger's physical operating conditions. No slip condition was applied on tube and fin wall surfaces. The walls of louvered fins and tubes were set at constant temperature boundary condition. Uniform velocity and temperature profiles were imposed at the inlet (blue zone) while the gage pressure of 0 Pa was applied at the exit (red zone) implying an atmospheric pres-

sure boundary condition. Periodic boundary conditions were applied to left-right (yellow zones), top-bottom sides (white) of the computational domain. Problem geometry dimensions and operating conditions are summarized in Table 1.

2.3. Validation of numerical model

The accuracy of the numerical model has been tested using experimental results of Wang et al. [33]. However, the heat transfer and pressure drop characteristics sensitively depend on the geometric structure. Therefore, it is not enough to set the same boundary conditions or provide similarity of the Reynolds number to compare the two cases. So, the geometric model representing the louvered fin and round tube heat exchanger of Wang et al. [33] was produced and numerical simulations were carried out at the same operating conditions as the experimental model with two tube rows and fin pitch of 2.08 mm. The friction f factors and Colburn j factors were calculated according to the procedure used by Wang et al. [34] for a more realistic comparison. Fig. 2 shows that the simulated results agree well with the experimental results with deviation of j-factor about 35% for lowest Reynolds number and about 12–8% for higher Reynolds numbers and deviation of f-factor about 40% for lowest Reynolds number and 12–4% for higher Reynolds numbers. This deviation range is acceptable for the purpose of this study. However, it would be more accurate to verify the numerical model with an experimental data conducted for an identical model. Therefore, the heat exchanger has been manufactured in accordance with the numerical model geometry and tested in the wind tunnel. In addition to this, a flow visualization experiment was performed with PIV and the simulation results and experimental results were compared.

Mesh independence study was carried out for the louvered fin and round tube heat exchanger for the largest louver angle of 30° for cases of present study. The mesh was refined starting from 2.35 to 21.76 millions of elements. Specifically, 2.35 million, 5.16 million, 8.2 million, 12 million and 21.76 million elements models were tested. The Colburn factor j and the friction f factor results were evaluated for the mesh independence study. The difference between the Colburn factor j values of 21.76 million elements model and those of 2.35 million, 5.16 million, 8.2 million and 12 million elements models were 3.1%, 0.5%, 0.01%, 0.0025%, respectively. The friction f factor results were converged for less number of elements. At least, a total of 12 million elements were used to solve the computational flow domain and the near-wall mesh with $y^+ = \rho u_T y/\mu \leqslant 1$ to compute heat flux more precisely. Here, u_T is the friction velocity defined as $u_T = \sqrt{\frac{\tau_w}{\rho}}$ which was utilized to resolve the viscous sublayer.

Finally the numerical model is validated with experimental results of Wang et al. [33], mesh independence study, PIV and wind tunnel experiments of the present study.

2.4. Data reduction for evaluating thermal and hydraulic performance

The airside heat transfer coefficient h_o can be calculated using Eq. (14)

$$h_o = \frac{\dot{Q}}{A_o \Delta T_m} \tag{14}$$

$$\Delta T_m = \frac{(T_w - T_{c,in}) - (T_w - T_{c,out})}{ln\left(\frac{(T_w - T_{c,in})}{(T_w - T_{c,out})}\right)} \tag{15}$$

Here, $\dot{Q}$, A_o, T_w and ΔT_m are the heat transfer rate, heat transfer surface area, the wall temperature and logarithmic mean temperature difference, respectively. The average Nusselt number is calculated by

$$\overline{Nu} = \frac{h_o H}{\lambda_a} \tag{16}$$

where H is the fin pitch and λ_a is the thermal conductivity of air. The Reynolds number based on the frontal air inlet velocity and fin pitch is defined as

$$Re = \frac{U_{frontal} H}{\nu} \tag{17}$$

The heat transfer characteristics are examined in terms of the Colburn factor j, relative Colburn factor j^* and the pressure drop characteristics in terms of friction factor f and relative friction factor f^* which are defined by

$$j = \frac{Nu}{RePr^{1/3}} \tag{18}$$

$$j^* = j/j_{ref} \tag{19}$$

$$f = \frac{\Delta p}{\rho \frac{U_{frontal}^2}{2} \frac{A_o}{A_c}} \tag{20}$$

and

$$f^* = f/f_{ref} \tag{21}$$

respectively.

Here, j_{ref} and f_{ref} are the Colburn factor and friction factor of plate fin and round tube heat exchangers, respectively.

Siddique et al. [35], Ferrero et al. [20] and Shevchuk et al.[36] used aerothermal efficiency to find a compromise between higher heat transfer enhancement and associated pressure losses. Similar to aerothermal efficiency, the thermal & hydraulic performance JF factor and relative JF^* factor were used and they can be defined by

$$JF = \frac{j}{(f)^{1/3}} \tag{22}$$

Table 1
Details of computational geometry and operating conditions.

Louver angle, θ (°)	22, 24, 26, 28, 30								
Flow length and Fin pitch ratio, F_l/H	20.625			26.4			31.428		
Louver pitch and Fin pitch ratio, L_p/H	0.843	1.093	1.187	1.080	1.400	1.52	1.285	1.666	1.809
Number of louvers	22	18	16	22	18	16	22	18	16
Longitudinal tube pitch and flow depth ratio P_l/F_L	0.5								
Transverse tube pitch and flow depth ratio P_t/F_L	0.5757								
Air frontal velocities $U_{frontal}$ (m/s)	1, 1.22, 1.50, 1.52, 1.75, 2, 2.25, 2.28, 3								
Air inlet temperature $T_{c,in}$ (°C)	20, 30								
Wall temperature T_w (°C)	40								

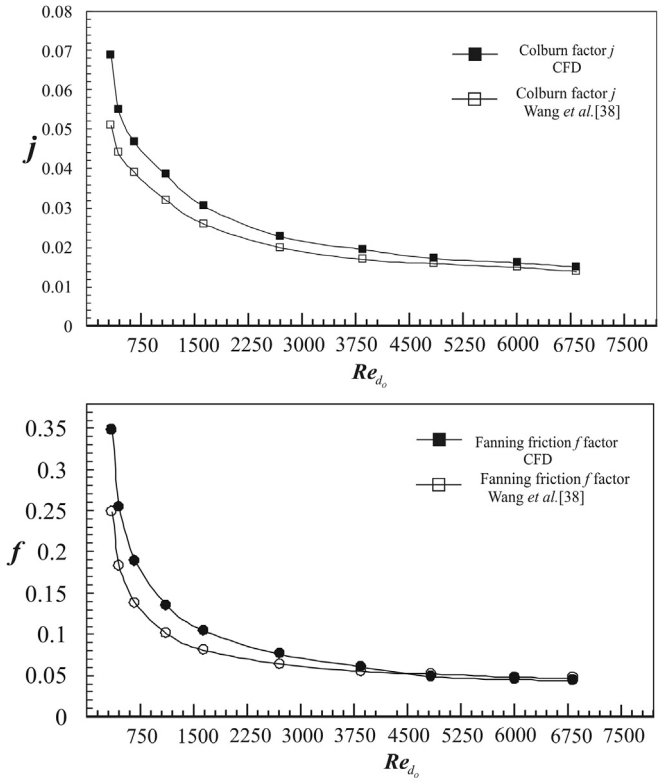


Fig. 2. Comparison of numerical and experimental results of Wang et al. [33] for cases of two tube rows and fin pitch of H = 2.08 mm.

and

$$JF^{*} = \frac{j/j_{ref}}{(f/f_{ref})^{1/3}} \tag{23}$$

respectively.

3. Experimental facility

3.1. PIV experiments

Experiments were performed in a large-scale open water channel with a rectangular cross-section. The dimensions of the water channel in the Advanced Technology Research and Application Centre of Selcuk University in Turkey were 770 mm, 600 mm and 6000 mm for width, height and length, respectively. The PIV system is depicted schematically in Fig. 3. Test-section walls were constructed from 15 mm thick transparent glass plates to simplify laser transmission and to provide flow visualization. The tank was filled with water to a level of h_w = 475 mm and the water was pumped by a centrifugal pump controlled with a frequency converter. The water passes through two honeycomb sections and a two-to-one channel contraction before reaching the test section. The uncertainty of free-stream turbulence intensity was less than 1% for the studied Reynolds numbers range. A Nd:YAG laser with a maximum frequency of 15 Hz was used to generate a laser sheet perpendicular to the axis of the splitters. The thickness of the laser sheet was approximately 1 mm. The 10 μm-diameter suspended silver-coated hollow glass sphere particles were used for seeding purposes in the flow. The interrogation area contains nearly 20–30 particles per image to fulfill the high-image density criterion. A Complementary Metal–Oxide–Semiconductor (CMOS) camera with a resolution of 1632 × 1200 pixels was utilized to capture 1024 instantaneous image pairs at a rate of 15 Hz. An interrogation window of 32 × 32 pixels for each image was selected and converted to approximately 1.41 × 1.41 mm^2 grid size (0.028L × 0.028L) with adaptive correlations consisting of 7474 (101 × 74) velocity vectors. During the adaptive-correlation process, an overlap of 50% was used for all interrogation areas to satisfy the Nyquist criterion. The time-averaged flow patterns were calculated from instantaneous velocity vector fields. Dantec Dynamic Studio software was employed for the post processing including proper filters to compute the raw displacement vector field from the particle image data. The laser was located below the splitters and face upwards while the CMOS camera was placed orthogonal to the laser and flow field as shown in Fig. 3. The time between two laser pulses was taken as 1750 ns to accurately catch the particle movement through the flow field. After body masking measurements, adaptive correlation and average filter processes were applied to obtain instantaneous and time average flow features.

The louvered fin model was built from transparent plexiglas material by a laser cutting and thermally shaping process and consisted of 15 rows of louvered fins which were enough to maintain periodic flow condition [37]. In the present study, the Reynolds number ($Re = (U_{frontal}\, H)/\nu$) is defined based on the characteristic length of the geometry and frontal velocity. Here, $U_{frontal}$ is the frontal velocity, H is fin pitch and υ is the kinematic viscosity of water. Fin pitch (H) and louver pitch (L_p) of the model are 32 mm and 35 mm, respectively.

3.2. Wind tunnel and conditioning room

The wind tunnel system is located in an isolated conditioned room. The air-side constant inlet conditions of temperature and humidity are maintained by the conditioning room which consists of an air handling unit; a refrigeration section, an electric heater with 18 kW power, a humidifier and three centrifugal fans to ensure adequate air recirculation in the system. The details of the experimental facility in the Friterm Inc. R&D laboratory are shown in Fig. 4.

The tested heat exchanger was placed at the inlet part of the suction type wind tunnel with a cross-section of 700 mm × 700 mm. The air inlet temperature and humidity are measured using an air sampler unit by thermocouples. The capacity measuring range for the heat exchanger is between 2.5 and 15 kW. The dry bulb temperature and relative humidity can be measured in the range of 0–45 °C and 40–100%, respectively. Air flow rate is measured in the flow rate measurement section using a nozzle by the pressure difference method. The air flow is supplied by a 7.5 kW centrifugal fan that can provide 500–7500 m^3/h volumetric flow rate and 0–1000 Pa pressure difference. The temperature, relative humidity and pressure of the outlet air are also measured in the mixing room.

Water was used as heat transfer fluid in the heat exchanger. The heat exchanger has inlet and outlet pipes which are used for charging and discharging water, respectively. Two sensors placed on these pipes were used to measure inlet and outlet temperatures and pressures for each pipe. The heat exchanger water flow was measured by a flow meter and a maximum of 5 m^3/h flow rate can be achieved with the pump setting. All experiments were repeated five times for repeatability purposes and average values were taken into account for analysis. The data received from the measurement devices were collected with serial bus by the data acquisition computer. Specifically, two Agilent 34970A data acquisition units collected most of the measured data such as air, water temperatures and air side pressure variation and transferred them to the computers. Measurement uncertainties of the instruments are given in Table 2.

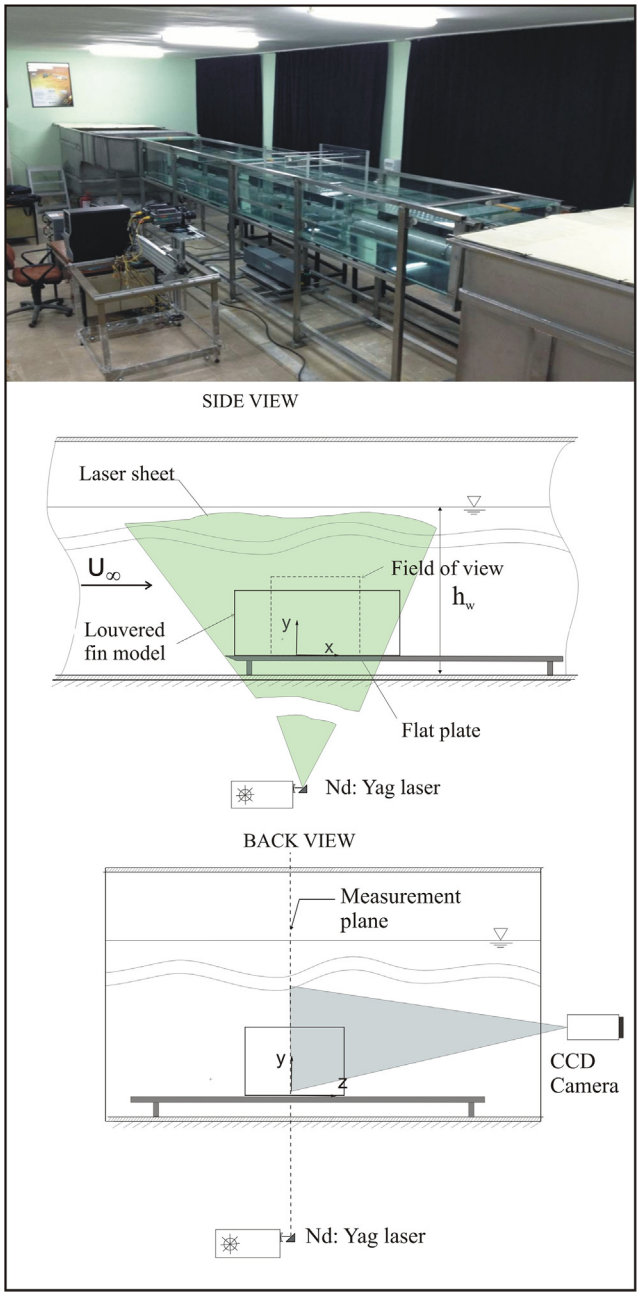


Fig. 3. Photo and schematic view of the PIV system experimental setup with laser illumination for the louvered fin model located in a uniform flow condition on a flat plate.

3.3. Data reduction

The air velocity was regulated with a 7.5 kW centrifugal fan at six constant free stream velocity values while the mass flow rate of water inside the heat exchanger tubes was kept at 4 m^3/h. The inlet temperatures of air and water were maintained at 20 °C and 40 °C, respectively.

The heat transfer rates for the air and water sides are obtained by this energy balance equations:

$$\dot{Q}_c = \dot{m}_c c_c.(T_{c,out} - T_{c,in}) \tag{24}$$

$$\dot{Q}_h = \dot{m}_h c_h.(T_{h,out} - T_{h,in}) \tag{25}$$

The value of the heat transfer rate is then taken as the average of air and water sides as

$$\dot{Q} = \frac{\dot{Q}_h + \dot{Q}_c}{2} \tag{26}$$

$$\dot{Q} = UA\Delta T_m \tag{27}$$

$$\Delta T_m = \frac{(T_{h,in} - T_{c,out}) - (T_{h,out} - T_{c,in})}{ln\left(\frac{(T_{h,in} - T_{c,out})}{(T_{h,out} - T_{c,in})}\right)} \tag{28}$$

The air-side heat transfer coefficient can be obtained from the heat transfer equation for cylindrical walls:

$$\frac{1}{UA} = \frac{1}{\eta_0 h_0 A_0} + \frac{\ln(d_o/d_i)}{2\pi\lambda_T L_T} + \frac{1}{h_i A_i}, \text{ in which} \tag{29}$$

The water-side heat transfer coefficient can be obtained from the Nu_i equation:

$$Nu_i = 0.023 Re_i^{0.8} \quad Pr^{0.3} \tag{30}$$

$$h_i = \frac{Nu_i \lambda_w}{d_i} \tag{31}$$

The surface efficiency is determined with the fin efficiency that is calculated using Schmidt approximation for the staggered plate-fin geometry [38]:

$$\eta_o = 1 - \frac{A_f}{A_o}(1 - \eta_f) \tag{32}$$

$$\eta_f = \frac{\tanh(mr\phi)}{mr\phi} \tag{33}$$

$$m = \sqrt{\frac{2h_o}{k_f \delta_f}} \tag{34}$$

$$\phi = \left(\frac{R_{eq}}{r} - 1\right)[1 + 0.35\ln(R_{eq}/r)] \tag{35}$$

To calculate the fin efficiency, the equivalent radius of the plate fin for circular fin for staggered tube layout is determined by [38]:

$$\frac{R_{eq}}{r} = 1.27\frac{X_M}{r}\left(\frac{X_L}{X_M} - 0.3\right)^{1/2} \tag{36}$$

$$X_L = \sqrt{\frac{(P_t/2)^2 + P_l^2}{2}} \text{ and } X_M = P_t/2 \tag{37}$$

4. Results and discussion

Thermal and hydraulic characteristics of the louvered fin and round tube heat exchangers obtained by numerical simulations in terms of relative Colburn factor j^*, relative friction factor f^* and relative JF^* depending on louver angle (θ), louver pitch to fin pitch ratio, (L_p/H) and Reynolds number for flow length to fin pitch ratios of F_l/H = 20.625, 26.4 and 31.428 are shown in Figs. 5–7, respectively. j^*, f^* and the JF^* are relative quantities which refer to the plate fin case as a reference. Temperature contours which were obtained from the middle cross-section plane (Visualization Plane A) of the first louver row at F_l/H = 31.428 are presented in Fig. 8.

4.1. j^*, f^* and JF^* factors for F_l/H = 20.625

A noticeable amount of heat transfer enhancement was obtained using louvered fins compared to flat plate fins depending on the louver angle, louver length and Reynolds number as shown in Fig. 5. An increasing in louver angle improves the mixture of cold

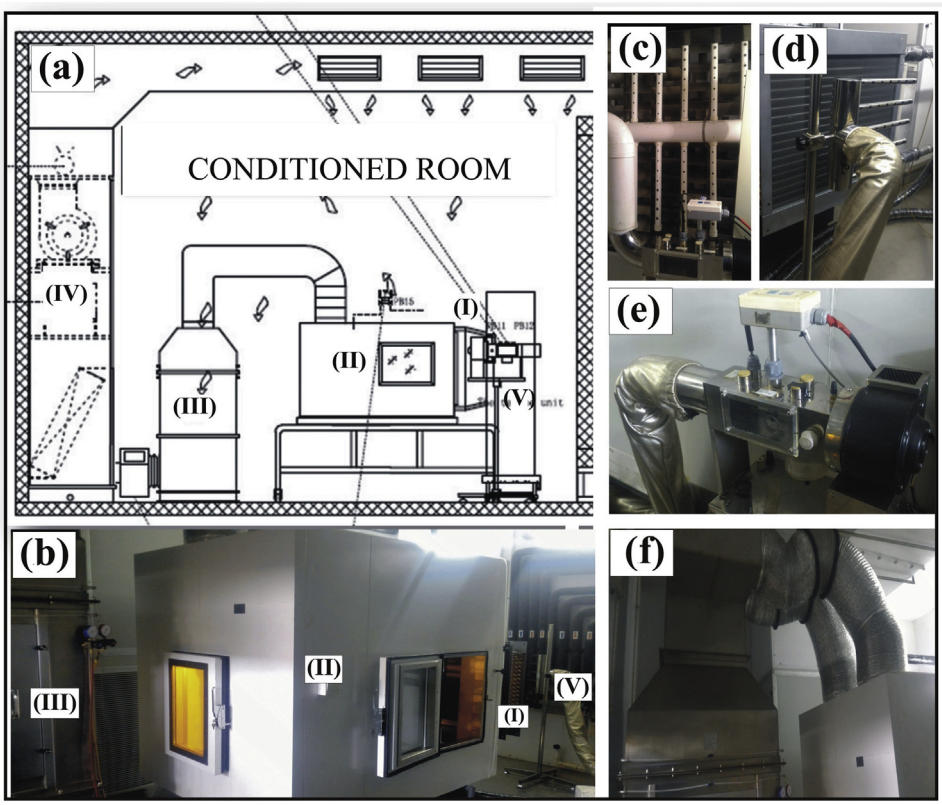


Fig. 4. Wind tunnel laboratory. (a) Schematic view (I) test object, (II) air receiver section, (III) flow rate measurement section, (IV) air handling unit, (V) air sampler, (b) photo of the conditioned room, (c) air sampler and temperature measurement box at outlet, (d) tested heat exchanger and air sampler at inlet (e) temperature measurement box at inlet and (f) connection of air receiver and flow measurement sections.

Table 2
Measurement uncertainties.

Measurement	Instrument	Location	Range	Uncertainties
Static pressure difference (air)	Yokogawa EJA110A	Inlet and outlet of product	(0)–(800) Pa	0.075%
Static pressure difference (nozzle)	Yokogawa EJA120A	Inlet and outlet of nozzles	(−50)–(450) Pa	0.15%
Temperature	Galltec	Temperature measurement box at inlet and outlet of product	(−40)–(85) °C	0.15 °C
Humidity	Galltec	Temperature measurement box at inlet and outlet of product	(0)–(100)% RH	1%
Temperature	PT 100	Water inlet and outlet of tubes	(−30)–(70) °C	0.1 °C
Flow rate	AXF025G Flow meter-FM3	Water flow rate in tubes	(0)–(5) m^3/h	0.5%

and hot fluids and therefore heat transfer enhancement is increased. Although a high amount of heat transfer improvement is obtained compared to the flat plate fins, the change due to the louver angle of the heat transfer enhancement is poor. Because of high fin pitch and low louver length, the ability of the louvers to direct the flow is relatively low. The implementation of the louvers with $L_p/H = 0.843$ and the louver angle 28° increases heat transfer by 158% and 146% compared with flat plate fins for the Reynolds numbers of 295 and 582, respectively.

The tendency of the louvers to direct the flow increases with the increase of the louver length. For this reason, there are considerable variations in the amount of heat transfer enhancement depending on the louver angle for $L_p/H = 1.093$ and 1.187. However, the increase in louver length leads to a thicker thermal boundary layer. Thus, when L_p/H ratio is increased to 1.093 and 1.187, the heat transfer enhancement in terms of j^* are reduced for all louver angles. Furthermore, the highest increase in heat transfer occurs for $L_p/H = 1.093$ when the louver angle becomes 30° while the lowest increase occurs when the louver angle is 26°. For $L_p/H = 1.187$, the maximum enhancement of heat transfer compared to the flat plate fins is obtained for the model with louver angle of $\theta = 30°$ (139% and 129% for Reynolds numbers of 295 and 582, respectively) while the minimum heat transfer enhancement is obtained for the model with a louver angle of $\theta = 24°$ (116–111%, for Reynolds number of 294.6 and 581.5, respectively). For this louver length, the increase of the louver angle also generally augments the heat transfer enhancement. However, the j^* factor of the case with louver angle of $\theta = 22°$ is larger than that of case with louver angle of $\theta = 24°$. This can be explained by the fact that the louvers differently orient the flow depending on their position to each other. For the louvered fins with $\theta = 24°$, the thermal wakes of the lower fins' louvers are oriented exactly in line with the upper fins' louvers, while the louvers with $\theta = 22°$ are less exposed to the effect of thermal wakes and the hot fluid and the cold fluid are better mixed. Similar flow structure and heat transfer mechanisms occur for $L_p/H = 1.187$.

As can be seen in Fig. 5, the pressure drop penalty in terms of f^* decreases with louver length (with L_p/H ratio) for all louver angles and increases with louver angle for all three louver lengths. The JF^* factor that takes into account the pressure drop and heat transfer enhancement together is an indication of the overall thermal and hydraulic performance of louvered fins and round tube heat

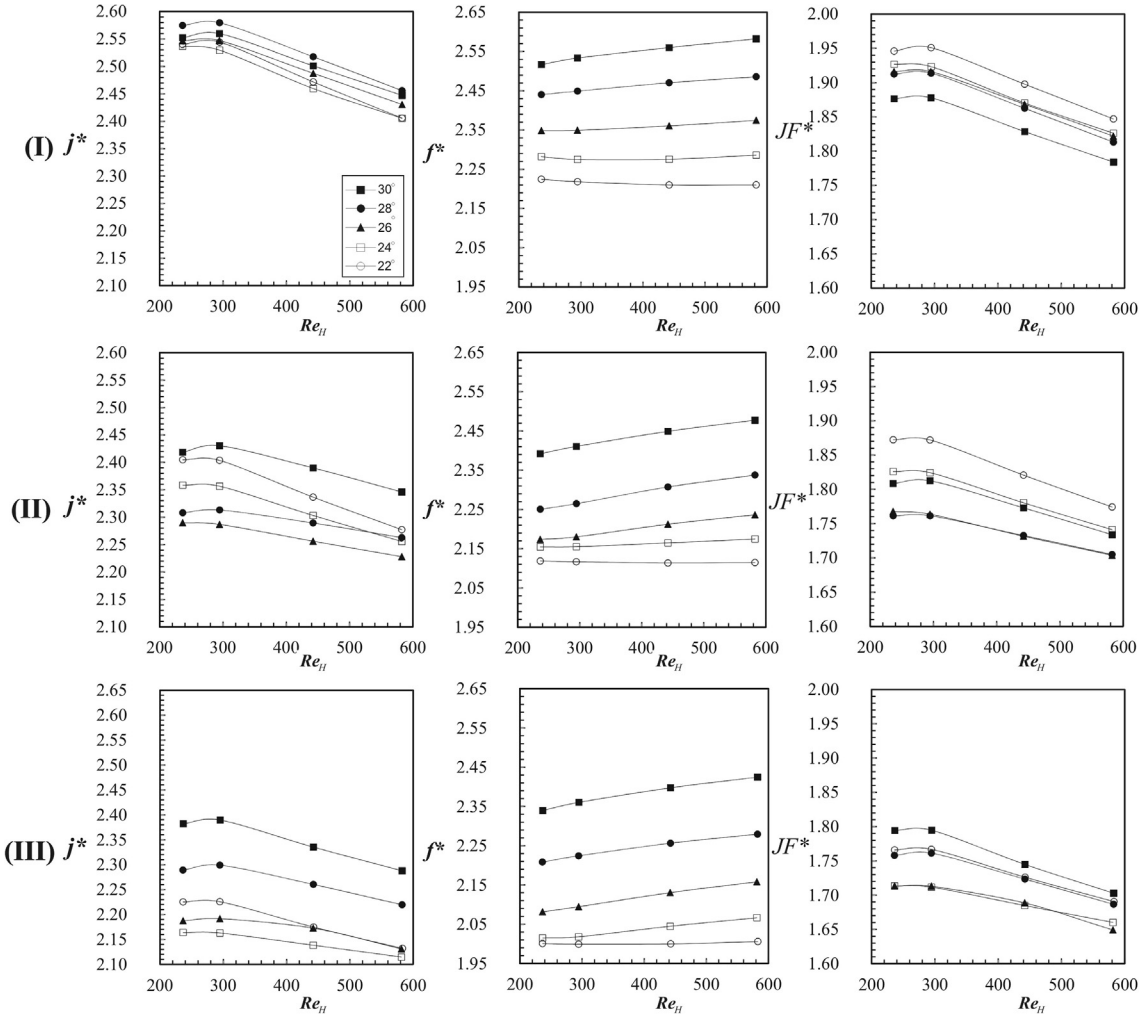


Fig. 5. The relative Colburn factor j^*, the relative friction factor f^* and JF^* plots at a ratio of flow length to fin pitch of F_L/H = 20.625 and ratios of louver pitch to fin pitch of L_p/H = 0.843 (row I), L_p/H = 1.093 (row II), L_p/H = 1.187 (row III).

exchangers. Increasing the Reynolds number decreases the JF^* values. The effect of louver angle on the JF^* factors is changed by louver length. The JF^* factor decreases with increasing louver angle for L_p/H = 0.843. For the case of L_p/H = 1.187, the maximum thermal–hydraulic performance is obtained for the louver angle of 30°.

4.2. j^*, f^* and JF^* factors for F_L/H = 26.4

The largest heat transfer enhancement about 153% is obtained for the louvered fin with louver angle of θ = 30° and L_p/H = 1.400 for Reynolds number of 345.3 as seen in Fig. 6. The effect of louver angle on heat transfer characteristics is poor for the louvered fins with L_p/H = 1.080 but larger for the louvered fins with L_p/H = 1.400 and L_p/H = 1.52. Pressure drop penalty characteristics in terms of the f^* factor values increase with louver angle while they decrease with louver lengths for all Reynolds numbers.

The louvered fins with θ = 30° create the highest heat transfer enhancement and j^* factor decreases with decreasing louver angle for the case of L_p/H = 1.400. This is due to the fact that the flow is completely louver directed and the thermal boundary layer can be continuously interrupted.

It can be concluded that the louver length and Reynolds number determine the effect of louver angle on thermal–hydraulic performance of the louvered fin and round tube heat exchangers. For L_p/H = 1.080, the louvers with angle of θ=22° showed the largest JF^* factors while the JF^* factors decreased with increasing louver angle. For L_p/H = 1.400, the largest JF^* factor was obtained for the louver angle of θ = 22° and θ = 30° for the Reynolds number of 185 and 455, respectively. Similar to this trend, for L_p/H = 1.52 at low Reynolds numbers, the louvered fin with 26° louver angle shows larger JF^* value while at larger Reynolds numbers the maximum JF^* values are obtained for the louvered fin with louver angle of 28°. For all cases, depending on Reynolds numbers, louver angles and louver lengths, overall thermal-hydraulic performances are increased between 63% and 88% using louvered fins.

4.3. j^*, f^* and JF^* factors for F_L/H = 31.428

Decreasing the fin pitch to this level causes significant variations on thermal and hydraulic behavior of the louvered fins depending on louver angle and length. It is easier that the flow forms to be louvered directed at low fin pitches configurations. Because when the fins are very close to each other, the flow tends to flow following the louvers instead of the duct. The more the air travels through the fins, the more the amount of heat transfer increases. However, if the louver positions allow the thermal boundary layer to thicken, the heat transfer rate starts to decrease. According to the j^* factor, an increase in heat transfer capacity

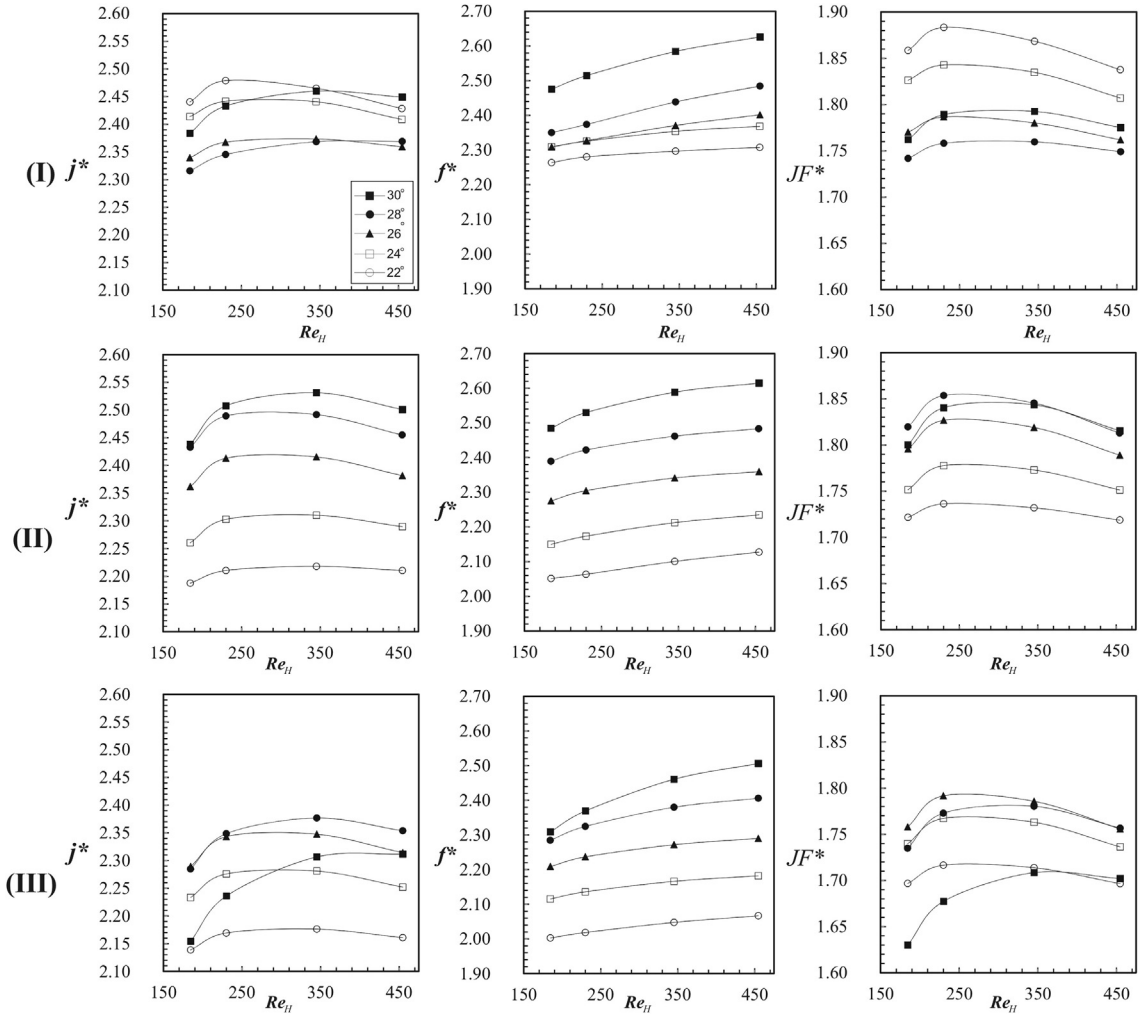


Fig. 6. The relative Colburn factor j^*, relative friction factor f^* and JF^* factor plots at the ratio of flow length to fin pitch F_L/H = 26.4 and ratios of louver pitch to fin pitch L_p/H = 1.080 (row I), L_p/H = 1.400 (row II), L_p/H = 1.52 (row III).

between 132% and 157% is obtained using louvers with the angle of 30° and L_p/H = 1.285 in the Reynolds number range between 147.6 and 363.2 as seen in Fig. 7. As can be seen from the temperature contours in Fig. 8, the position of the louvers also does not allow the thickness of the thermal boundary layer to increase as the louver angle increases for the case L_p/H = 1.285. As a result, as the louver angle increases, the air flow distance in the heat exchanger extends and the enhancement in heat transfer increases. The lowest enhancement is obtained for the case of the louvered fin with a louver angle of 22°. When the ratio of the louver length to the fin pitch increases to L_p/H = 1.666, the thermal boundary layer thickness changes with respect to the louver angle as seen in Fig. 8. In this case, contrary to what is expected, the increase in the distance where the air traveled between the fins does not increase the heat transfer enhancement. When the louver angle is kept constant at 30° and L_p/H ratio is increased to 1.666, the j^* factors decrease about 32.32% and 30.35% at Reynolds numbers of 148 and 363, respectively compared to louvered fin with L_p/H = 1.285. Moreover, the heat transfer capacity levels of all models are changed and the louvered fin with louver angle of 30° exhibits the lowest heat transfer enhancement. On the other hand, the louvered fin with louver angle of 24° provides the highest heat transfer enhancement. Increasing the louver length caused an increase in heat transfer enhancement capacity of the louvered fins with smaller louver angles such as 22° and 24° while heat transfer capacities of louvers with the louver angle of 26°, 28° and 30° are weakened with louver length. When the L_p/H ratio increases from 1.666 to 1.809, heat transfer enhancement characteristics significantly decrease for all louver angles. When the L_p/H ratio is increased from 1.285 to 1.809, the heat transfer enhancement percentages decrease from 127% to 123%, from 131% to 119%, from 139% to 99%, from 150% to 69%, from 157% to 60% for louver angles of 22°, 24°, 26°, 28° and 30°, respectively. For L_p/H = 1.809, the amount of heat transfer enhancement decreases as the louver angle increases. As can be seen from the temperature contours in Fig. 8, interrupting the thermal boundary layer is completely reduced, especially for the fins with θ = 30° louvers. Increasing the louver angle to 30° makes the distance of the leading edge and trailing edge of upper and lower fins' louvers come closer at a small fin pitch. Although the flow length is extended, thermal boundary layer is thicker when the fluid flows along the louvers across the fins since the louver angle is larger. In such a configuration, the boundary layer flow cannot mix with the main flow to be interrupted and restarted due to fact that there is not enough flow path distance for this process.

It should be noted that the influence of louver angle on the pressure drop penalty depends on the louver length for this small fin pitch. As explained above, the distance of the leading edge and trailing edge of the upper and lower fins' louvers changes with louver angle. For larger L_p/H ratios of 1.666 and 1.809, a straight flow

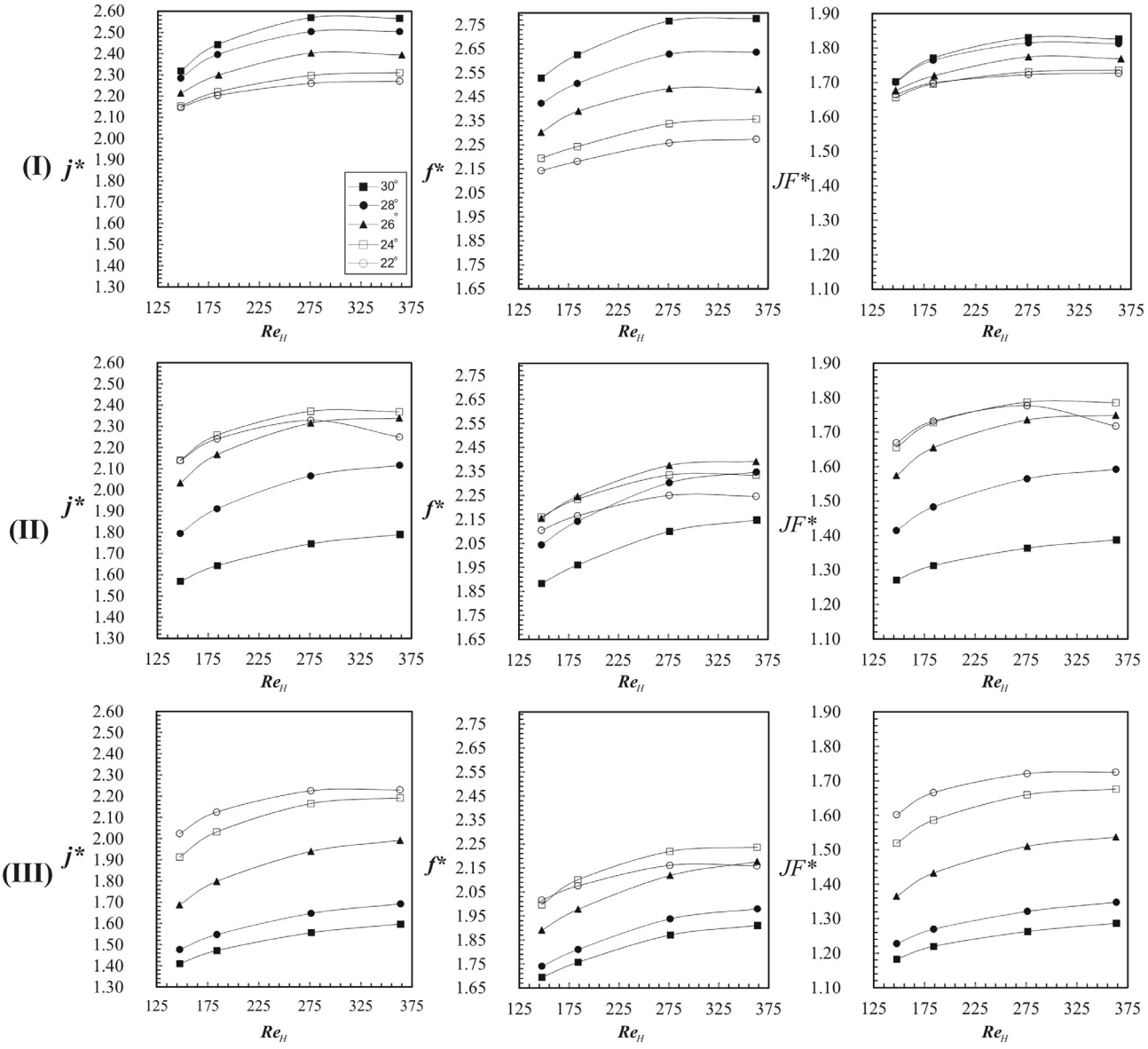


Fig. 7. The relative Colburn factor j^*, the relative friction factor f^* and JF^* factor plots at the ratio of flow length to fin pitch F_l/H = 31.428 and ratios of louver pitch to fin pitch L_p/H = 1.285 (row I), L_p/H = 1.666 (row II), L_p/H = 1.809 (row III).

path without mixing of the boundary layer forms and friction effects are reduced. Hence, for L_p/H = 1.285, the f^* factors increase with louver angle for all Reynolds numbers while there are more complicated relations between pressure drop penalty and louver angle for the cases L_p/H = 1.666 and 1.809 as given in Fig. 7. The louvered fin and round tube heat exchanger with louver angle of 30° and L_p/H = 1.285 causes the largest pressure penalty while the pressure drop penalty of the model with louver angle of 30° significantly decreases to the smallest value for larger L_p/H ratios of 1.666 and 1.809. Generally, increasing the louver length for a certain louver angle decreases the pressure drop penalty at different rates depending on the louver angle.

As seen in Fig. 7 (column III), the thermal-hydraulic performance in terms of JF^* factors increases as the L_p/H ratio increases from 1.285 to 1.666 for louver angles of 22° and 24° while JF^*-reduces for louver angles of 26°, 28° and 30°. Increasing L_p/H ratio to 1.809 causes large reductions on the thermal-hydraulic performance of the heat exchanger models with louver angles of 24°, 26°, 28° and 30°. However, the model with louver angle of 22° reaches the largest thermal-hydraulic performance by increasing L_p/H to 1.809. At large Reynolds numbers, the air flows as louver-directed with a thinner boundary layer while at low Reynolds numbers the air flows through the duct and this flow is called duct-directed flow with a thicker boundary layer and high flow resistance that is caused by louvers. This means that at low Reynolds numbers louvers largely cause pressure drops without any noticeable heat transfer enhancement. Higher thermal-hydraulic performance at high Reynolds numbers for larger louver angles can be attributed to this situation.

4.4. PIV and performance test results

Flow characteristics such as patterns of sectional streamlines and velocity vectors obtained using the PIV technique and the CFD for Reynolds number of 1783 and a raw image of PIV measurements are shown in Fig. 9. Four measurement planes were used to visualize the flow pattern of the full model and the model with the largest fin pitch of H = 32 mm (L_p/H = 1.093) (10 times scaled up of

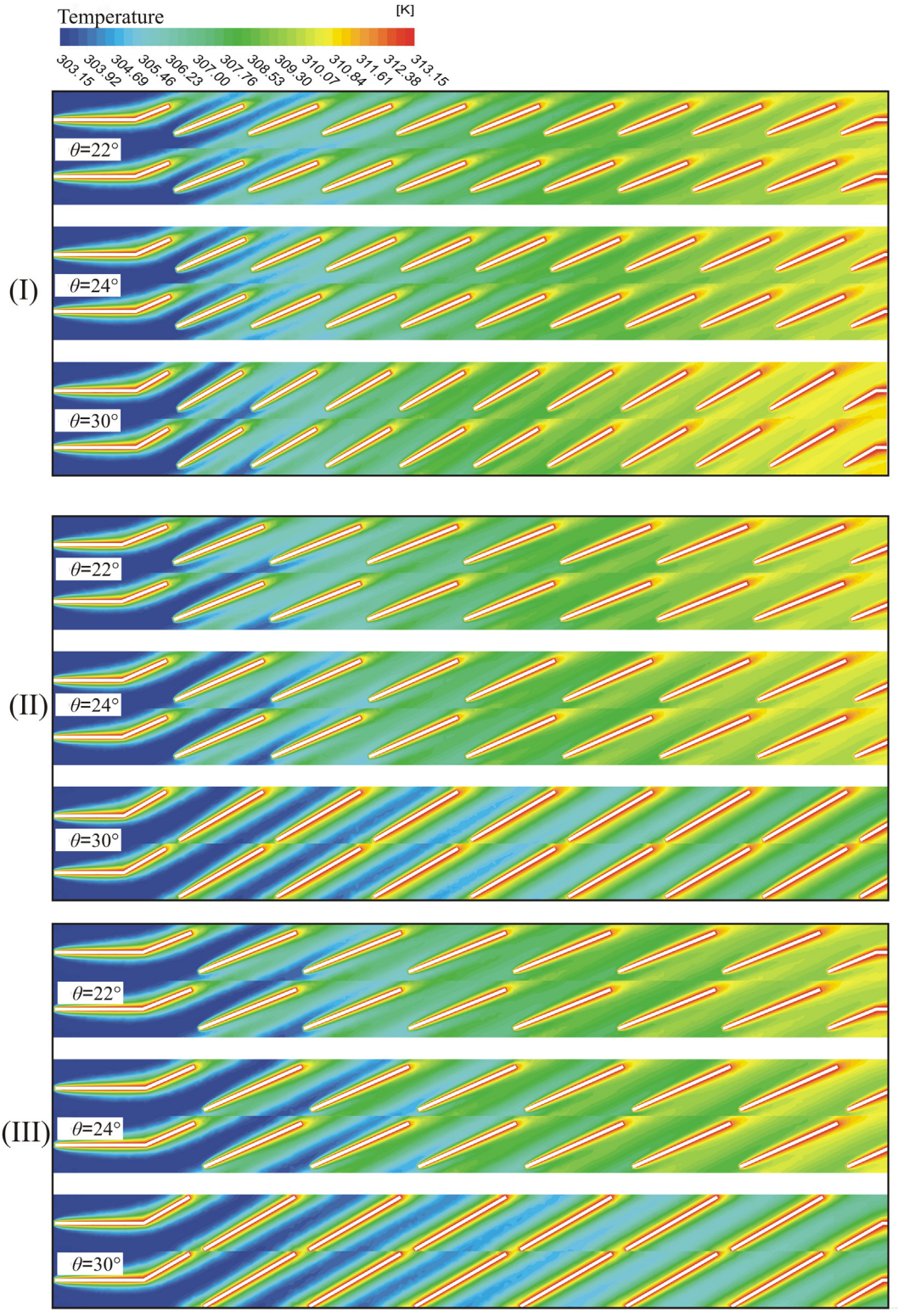


Fig. 8. Temperature contours which are obtained from the middle cross-section plane (Visualization Plane A) of the first louver row at a ratio of flow length to fin pitch of F_l/H = 31.428 and ratios of louver pitch to fin pitch L_p/H = 1.285 (row I), L_p/H = 1.666 (row II), L_p/H = 1.809 (row III) for $U_{frontal}$ = 3 m/s.

the real size heat exchanger) was selected to conduct PIV measurements. It was noted that enlarging the fin pitch causes the fluid to flow through the duct which is called duct-directed flow. In a good design of louvered fin, the flow is louvered-directed and the fin has high thermal and hydraulic performance. Testing the largest fin pitch is reliable enough to ensure that flow is louvered-directed. CFD simulations were performed to validate the turbulence model as well as to increase the reliability of PIV results. The streamlines and velocity vectors give the necessary information about the flow around the louvered fins. It is observed that the flow is completely louver-directed based on streamlines obtained from both numerical analysis and PIV measurements. When the velocity vectors are

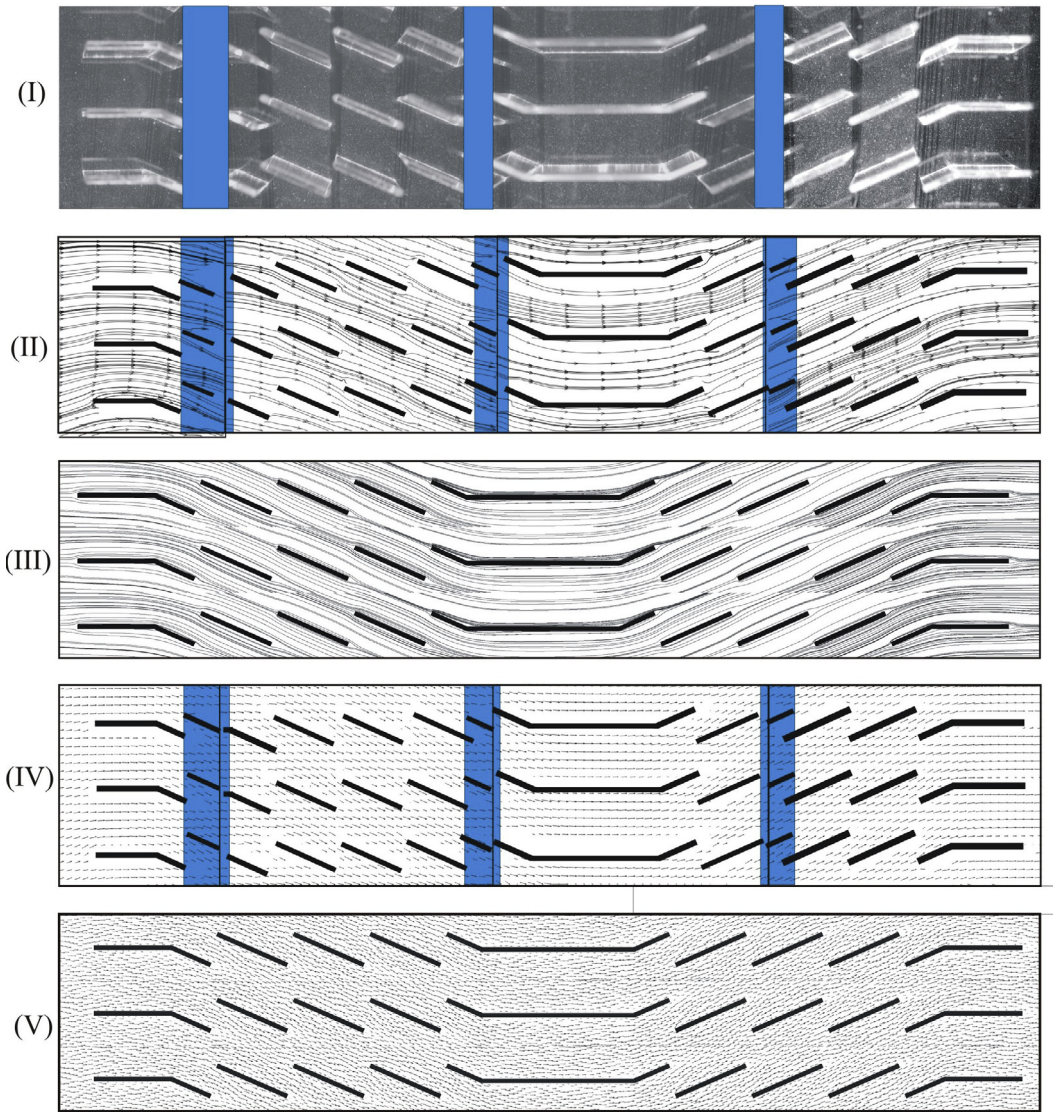


Fig. 9. Raw PIV image (row I), patterns of time averaged streamlines (raw II experimental, raw III numerical), velocity vector maps (raw IV experimental, raw V numerical) for louver angle $\theta = 24^\circ$ and ratio of louver pitch to fin pitch $L_p/H = 1.093$.

taken into consideration, it is found that while the flow is louver-directed, there is no flow separation around the louvers. Flow separation does not add any contribution to the heat transfer, but it is an effect that causes an increase in pressure drop by reducing the amount of heat transfer. Velocity vectors and streamlines give nearly the same results in numerical siumations and PIV measurements. However, these measurements were performed at a higher Reynolds number than the heat exchanger's operating conditions. While the Reynolds number increases in the louvered fin heat exchangers, the tendency of the flow to follow the louvers increases. Therefore, more experiments should be conducted for low Reynolds numbers, too.

For validation of the numerical model, a louvered fin model with louver angle of $\theta = 24^\circ$ and $L_p/H = 1.400$ for $F_L/H = 26.4$ ($L_p/H = 1.093$ for $F_L/H = 20.625$ and $Lp/H = 1.666$ for $F_L/H = 31.428$) was selected to manufacture. When the values of j^* and JF^* above are examined, it can be seen that this model has a high thermal - hydraulic performance.

Before deciding to manufacture the real size prototype, flow visualization of the CFD simulations were evaluated in more detail. Fig. 10 illustrates temperature contours obtained from the top periodic plane, streamline patterns and temperature contours taken from cross-section planes in the middle of inlet and outlet louvers and local Nusselt number contours over louvered fin for $F_d/H = 26.4$, $L_p/H = 1.400$, $\theta = 24^\circ$ and frontal air velocity of 2.5 m/s. As it can be seen from the streamline patterns, the flow is louver-directed. In the end of the inlet louver region and upstream of the tubes, a large recirculation region patterns of a horseshoe vortex is formed. Sahin et al. [39] experimentally showed the formation of horseshoe vortexes for plate fin and tube heat exchangers via PIV technique. They reported that horseshoe vortexes magnify the entrainment process which occurs between the main flow and the wake-flow regions and enhances the heat transfer rate in the case of fin-tube heat exchangers. In the upstream region of the outlet louvers, wake region of the tubes are formed. This disrupts the flow to obstruct the louvers; however, the flow develops after two-three louvers and starts to follow louvers again. The temperature distribution along the louvers and local Nusselt number distribution over louvered fin give considerable information about heat transfer characteristics. The heating process of cold fluid along the louvers and mixing of cold and hot fluids can be easily observed. Therefore, the selected model is a good design example for the current operating conditions.

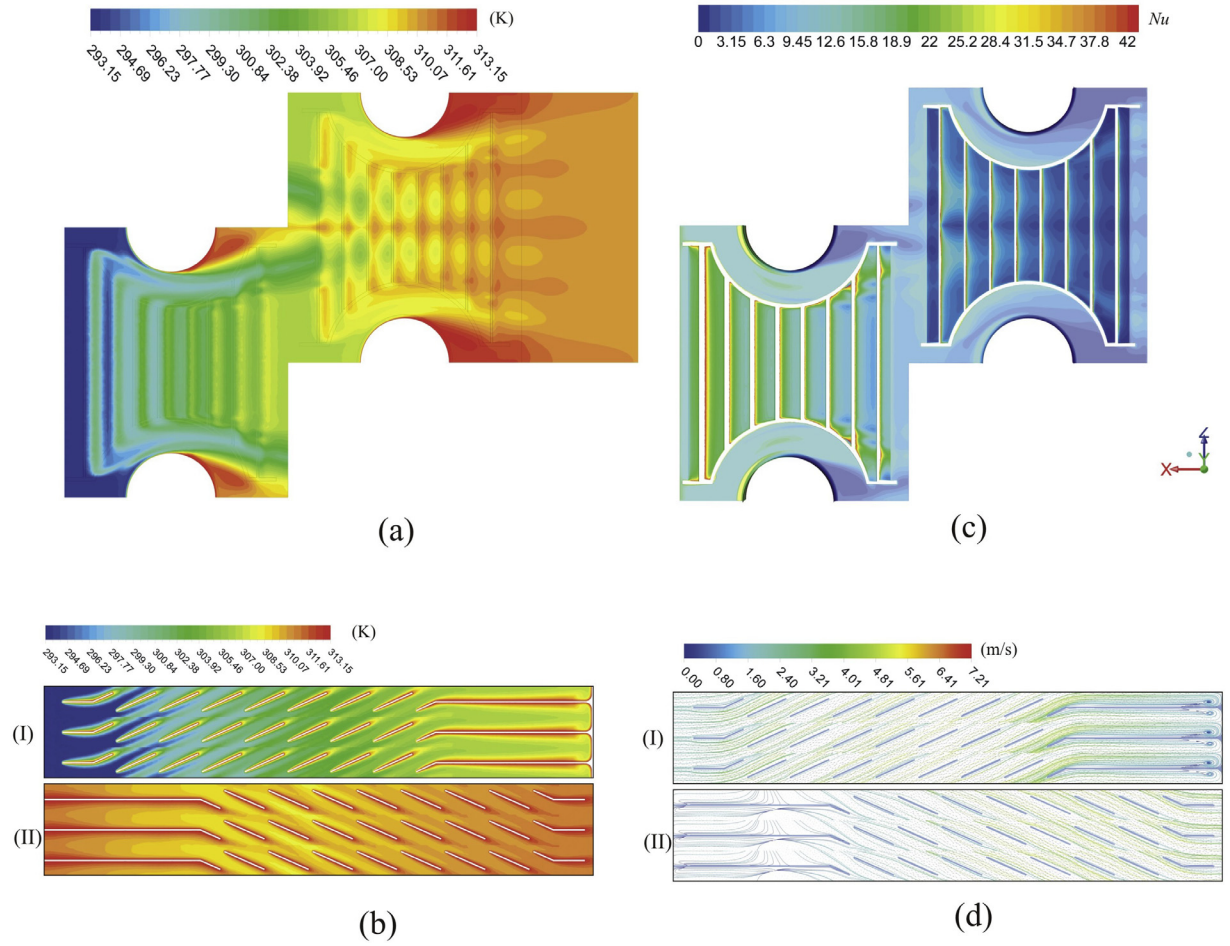


Fig. 10. Temperature contours which are obtained from top periodic plane (a) and (b) the middle cross-section plane of the first louver row (Visualization Plane A) (I) and louver row (Visualization Plane B) (II). (c) Local Nusselt number contours over louvered fin. (d) Streamline patterns and velocity vectors which are obtained from the middle cross-section plane of the first louver row (Visualization Plane A) (I) and second louver row (Visualization Plane B) (II), for $\theta = 24°$, $F_l/H = 26.4$ and $L_p/H = 1.400$ and frontal air velocity of 2.5 m/s.

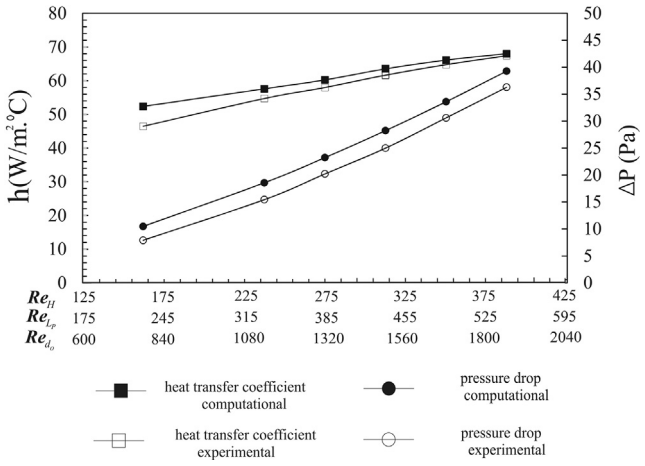


Fig. 11. Comparison of numerical and experimental results for $\theta = 24°$, $F_l/H = 26.4$ and $L_p/H = 1.400$.

In Fig. 11, the numerical simulation and experimental results are compared for different air Reynolds numbers. It was found that the pressure drop and heat transfer coefficient obtained with the numerical study are in good agreement with the experimental results. The pressure drops obtained from the experiments somewhat exceeded the numerical results, but this is an acceptable difference. Prototypes of models used in the numerical analysis have been manufactured using aluminum fin and copper tubes and tested in the wind tunnel.

Experimental results of the thermal and hydraulic characteristics of the louvered fin and round tube heat exchanger ($F_l/H = 26.4$ and $L_p/H = 1.400$ and $\theta = 24°$) and a wavy fin and round tube heat exchanger in terms of Colburn factor j, friction factor f and JF factor are given in Fig. 13. The wavy fin and round tube heat exchanger has identical dimensions with the louvered fin and tube heat exchanger and the schematic view of wavy fin is shown in Fig. 12. Table 3 gives the test conditions and corresponding measurement results.

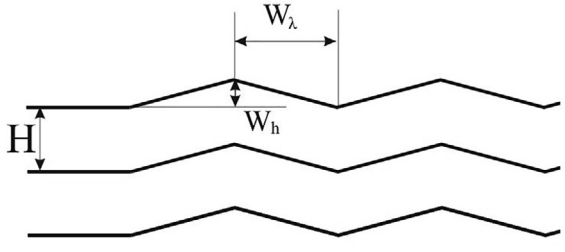


Fig. 12. Schematic view of wavy fin. $F_l/H = 26.4$, $W_h/H = 0.4$, $W_\lambda/H = 1.5$.

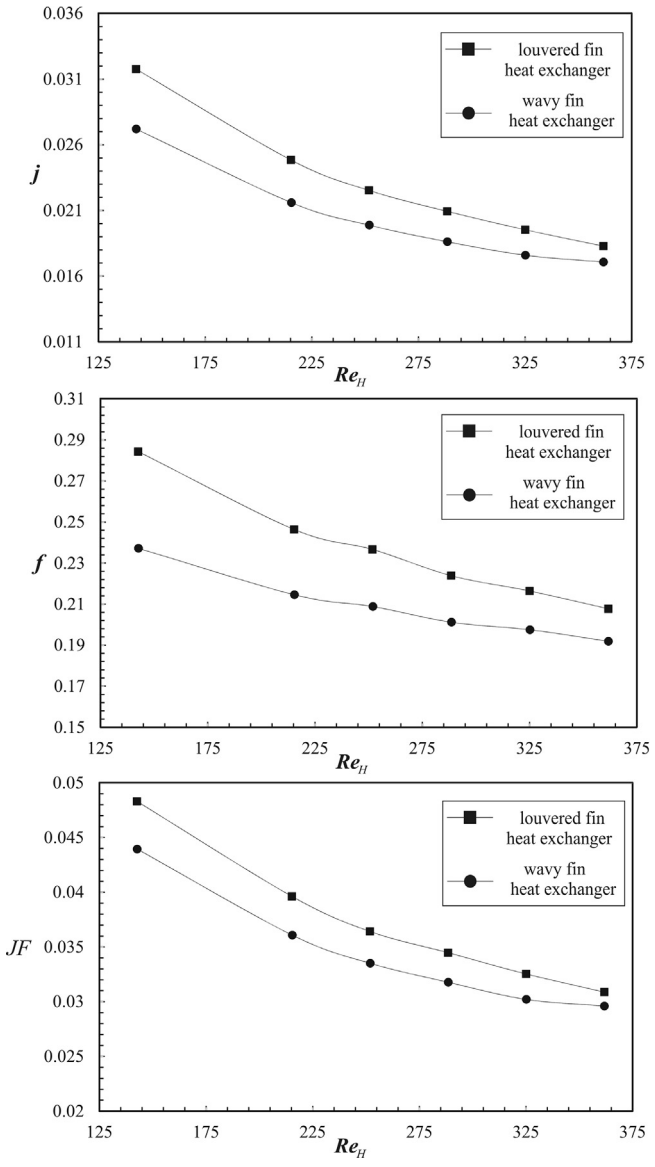


Fig. 13. Comparison of experimental results for louvered fin and round tube heat exchanger (θ = 24°, F_l/H = 20.625 and L_p/H = 1.093) and wavy fin and round tube heat exchanger (F_l/H = 20.625, W_h/H = 0.44, W_s/H = 1.66).

The Colburn factors j of the louvered fin and round tube heat exchanger are larger than that of the wavy fin and round tube heat exchanger about 16.8% and 7% for the lowest and highest Reynolds numbers, respectively as a result of heat transfer enhancement. On the other hand, the friction factors f increase between 19.9% and 8.2% compared to the wavy fin case. Similar to louvered fins, wavy fins increase flow length due to their geometry and besides increasing heat transfer surface area, wavy fins increase convection heat transfer coefficient and pressure drop penalties compared to flat plate heat exchangers. Wavy fins can produce vortices which enhance mixing of air. As a result, thermal boundary layer growth is weakened and heat transfer is enhanced. However, the louvered fin and round tube heat exchanger has a larger heat transfer performance and pressure drop penalties than the wavy fin and round tube heat exchanger. The reason of this situation can be explained as follows. As mentioned before, wavy fins extend the flow path; however, the air can still flow only between two fins without mixing air that flows between other fins. In the case of the louvered fin heat exchangers, the air can flow across the different fins depending on the louver angle, providing a better mixing.

The JF factors, which consider both the pressure drop penalty and the heat transfer enhancement together, are higher for the louvered fin and round tube heat exchanger than that for the wavy fin and round heat exchanger, about 10% - 4.3%. Therefore, the new designed louvered fin and round tube heat exchanger is superior to the wavy fin and round tube heat exchanger in terms of thermal and hydraulic performance.

5. Conclusions

In this study numerical simulations were performed with different louver angles, louver lengths (pitches), fin pitches and operating conditions in order to determine heat transfer and pressure drop characteristics. The obtained results are presented as relative Colburn factor j^*, friction factor f^* and JF^*, which characterize heat transfer, pressure drop and thermal & hydraulic performance, respectively. PIV measurements were then conducted for flow visualization and validation of CFD model purposes and the results were presented as velocity vectors and streamlines. A louvered fin and round tube heat exchanger prototype was manufactured and the heat transfer coefficients and pressure drop were measured in a wind tunnel that was located in a conditioning room. The heat transfer and pressure drop characteristics of the louvered fin and round tube heat exchanger were compared to that of a wavy fin

Table 3
Experimental parameters and measurements for louvered fin and round tube heat exchanger and wavy fin and round tube heat exchanger.

Test number (Louvered fin heat exchanger)	Air volumetric flow rate (m^3/h)	Water volumetric flow rate (m^3/h)	Air frontal velocities $U_{frontal}$ (m/s)	Air side pressure drop (Pa)	Fluid side pressure drop (kPa)	Air inlet temperature $T_{c,in}$ (°C)	Air outlet temperature $T_{c,out}$ (°C)	Water inlet temperature $T_{h,in}$ (°C)	Water outlet temperature $T_{h,out}$ (°C)
1	1765.27	4.00	1.00	7.88	22.31	20	33.51	39.97	38.20
2	2648.85	4.00	1.50	15.42	22.26	20	31.35	39.97	37.78
3	3092.87	4.00	1.75	20.19	22.32	20	30.45	39.96	37.60
4	3535.24	4.00	2.00	24.98	22.28	19.97	29.64	40.03	37.44
5	3972.91	4.00	2.25	30.59	22.31	20	29.07	40.04	37.31
6	4411.91	4.00	2.50	36.28	22.39	19.99	28.53	39.98	37.17
(Wavy fin heat exchanger)									
1	1765.70	4.00	1.00	6.58	22.66	20.01	32.81	40	38.33
2	2650.59	4.00	1.50	13.44	22.65	20.01	30.73	39.99	37.92
3	3091.05	4.00	1.75	17.83	22.64	20	29.93	39.99	37.74
4	3534.76	4.00	2.00	22.46	22.62	20	29.3	39.98	37.58
5	3976.33	4.00	2.25	27.93	22.65	20.01	28.76	39.97	37.42
6	4419.78	4.00	2.50	33.52	22.58	20.02	28.43	40	37.32

and round tube heat exchanger with identical size and specifications. The findings can be summarized as follows:

- The increase of j^* and JF^* values with the Reynolds number is due to the tendency of the flow to orient along the louvers at relatively high Reynolds numbers.
- For $F_d/H = 20.625$ and all louver lengths, heat transfer enhancement is generally higher for larger louver angles and pressure drops increases with louver angle. The increase in the length of the louvers increases the effect of louver angles on the heat transfer enhancement.
- When the ratio of the flow length to the fin pitch is increased to $F_p/H = 26.4$ (when the fin pitch decreases) f^*factors increase with louver angle for all louver lengths. j^* factors regularly increase with louver angle for $L_p/H = 1.400$ while they change irregularly with louver angles for $L_p/H = 1.080$ and 1.52.
- When the fin pitch is at the lowest level ($F_d/H = 31.428$) j^* factors start to decrease with the louver angle for louver pitch and fin pitch ratios of $L_p/H = 1.66$ and 1.809.
- For the $F_L/H = 20.625$, the highest thermal-hydraulic performances in terms of JF^* *at* Lp/H ratios of 0.843, 1.093 and 1.187 were obtained for louver angles of 22°, 22° and 30°, respectively. The highest JF^* values were obtained among these cases for the model with $Lp/H = 0.843$ and louver angle of 22°.
- For $F_L/H = 26.4$, the highest thermal-hydraulic performances in terms of JF^* at Lp/H ratios of 1.080, 1.400 and 1.520 were obtained for louver angles of 22°, 28° and 26°, respectively. The highest JF value was obtained among these cases for the model with $F_L/H = 1.080$ and louver angle of 22°.
- For $F_L/H = 31.428$, the highest thermal-hydraulic performances in terms of JF^* at Lp/H ratios of 1.285, 1.666 and 1.809 were obtained for louver angles of 30°, 24° and 22°, respectively. The highest JF^* values were obtained among these cases for the model with $Lp/H = 1.285$ and louver angle of 30°. The JF^* values of the model with $Lp/H = 1.285$ and $\theta = 24°$ are also close to the values of the model with $Lp/H = 1.285$ and $\theta = 30°$.
- When PIV and CFD results are compared, there is good agreement between them. When the streamlines lines and velocity vectors are examined, it is seen that the flow is louver-directed and the fin has high thermal-hydraulic performance. In tests carried out in the wind tunnel, the pressure drop and heat transfer characteristics are in good agreement with CFD results.
- The Colburn factor *j*, Fanning friction factor *f* and *JF* factor of the louvered fin heat exchanger are higher than that of the wavy fin heat exchanger, about 16.8–7%, 19.9–8.2% and 10–4.3% depending on the Reynolds number, respectively

Acknowledgments

This research has been performed under the Industrial Thesis Project contract number of 0649.STZ.2014. The authors would like to acknowledge the funding of Republic of Turkey Ministry of Science, Industry and Technology and FRITERM Company. Also, thanks to R&D Engineers Dr. Hüseyin Onbaşıoğlu, Mete Özşen and Mehmet Harun Sökücü who have cooperated in the manufacturing and testing of the heat exchangers.

References

[1] M.E. Springer, K.A. Thole, Experimental design for flowfield studies of louvered fins, Exp. Therm. Fluid Sci. 18 (3) (1998) 258–269.
[2] A.C. Lyman, R.A. Stephan, K.A. Thole, L.W. Zhang, S.B. Memory, Scaling of heat transfer coefficients along louvered fins, Exp. Therm. Fluid Sci. 26 (5) (2002) 547–563.
[3] N.C. DeJong, A.M. Jacobi, Flow, heat transfer, and pressure drop in the near-wall region of louvered-fin arrays, Exp. Therm. Fluid Sci. 27 (3) (2003) 237–250.
[4] C. T'Joen, A. Jacobi, M. De Paepe, Flow visualisation in inclined louvered fins, Exp. Therm. Fluid Sci. 33 (4) (2009) 664–674.
[5] H. Huisseune, C. T'Joen, P. De Jaeger, A. Willockx, M. De Paepe, Study of junction flows in louvered fin round tube heat exchangers using the dye injection technique, Exp. Therm. Fluid Sci. 34 (8) (2010) 1253–1264.
[6] C.C. Wang, Y.T. Lin, C.J. Lee, Heat and momentum transfer for compact louvered fin-and-tube heat exchangers in wet conditions, Int. J. Heat Mass Transf. 43 (18) (2000) 3443–3452.
[7] M.H. Kim, C.W. Bullard, Air-side thermal hydraulic performance of multi-louvered fin aluminum heat exchangers, Int. J. Refrig. 25 (3) (2002) 390–400.
[8] Z. Qi, J. Chen, Z. Chen, Parametric study on the performance of a heat exchanger with corrugated louvered fins, Appl. Therm. Eng. 27 (2) (2007) 539–544.
[9] A. Vaisi, M. Esmaeilpour, H. Taherian, Experimental investigation of geometry effects on the performance of a compact louvered heat exchanger, Appl. Therm. Eng. 31 (16) (2011) 3337–3346.
[10] B. Dogan, Ö. Altun, N. Ugurlubilek, M. Tosun, T. Sariçay, L.B. Erbay, An experimental comparison of two multi-louvered fin heat exchangers with different numbers of fin rows, Appl. Therm. Eng. 91 (2015) 270–278.
[11] M.H. Shojaeefard, J. Zare, Modeling and combined application of the modified NSGA-II and TOPSIS to optimize a refrigerant-to-air multi-pass louvered fin-and-flat tube condenser, Appl. Therm. Eng. 103 (2016) 212–225.
[12] B. Torregrosa-Jaime, J.M. Corberan, J. Paya, J.L. Delamarche, Thermal characterisation of compact heat exchangers for air heating and cooling in electric vehicles, Appl. Therm. Eng. 115 (2017) 774–781.
[13] K.N. Atkinson, R. Drakulic, M.R. Heikal, T.A. Cowell, Two- and three-dimensional numerical models of flow and heat transfer over louvred fin arrays in compact heat exchangers, Int. J. Heat Mass Transf. 41 (24) (1998) 4063–4080.
[14] T. Perrotin, D. Clodic, Thermal-hydraulic CFD study in louvered fin-and-flat-tube heat exchangers, Int. J. Refrig. 27 (4) (2004) 422–432.
[15] J.S. Leu, M.S. Liu, J.S. Liaw, C.C. Wang, A numerical investigation of louvered fin-and-tube heat exchangers having circular and oval tube configurations, Int. J. Heat Mass Transf. 44 (22) (2001) 4235–4243.
[16] J. Jang, Y. Tsai, Optimum louver angle design for a louvered fin heat exchanger, Int. J. Phys. Sci. 6 (28) (2011) 6422–6438.
[17] V.P. Malapure, S.K. Mitra, A. Bhattacharya, Numerical investigation of fluid flow and heat transfer over louvered fins in compact heat exchanger, Int. J. Therm. Sci. 46 (2) (2007) 199–211.
[18] C.T. Hsieh, J.Y. Jang, Parametric study and optimization of louver finned-tube heat exchangers by Taguchi method, Appl. Therm. Eng. 42 (2012) 101–110.
[19] J.N. Mao, H.X. Chen, H. Jia, Y.Z. Wang, H.M. Hu, Effect of air-side flow maldistribution on thermalehydraulic performance of the multi-louvered fin and tube heat exchanger, Int. J. Therm. Sci. 73 (2013) 46–57.
[20] M. Ferrero, A. Scattina, E. Chiavazzo, F. Carena, D. Perocchio, M. Roberti, G. Toscano Rivalta, P. Asinari, Louver finned heat exchangers for automotive sector : numerical simulations of heat transfer and flow resistance coping with industrial constraints, ASME J. Heat Transfer 135 (12) (2013).
[21] B. Ameel, J. Degroot, C. T'Joen, P. De Jaeger, H. Huisseune, S. De Schampheleire, J. Vierendeels, M. De Paepe, Optimization of X-shaped louvered fin and tube heat exchangers while maintaining the physical meaning of the performance evaluation criterion, Appl. Therm. Eng. 58 (1–2) (2013) 136–145.
[22] P. Karthik, V. Kumaresan, R. Velraj, Experimental and parametric studies of a louvered fin and flat tube compact heat exchanger using computational fluid dynamics, Alex. Eng. J. 54 (4) (2015) 905–915.
[23] F. Sangtarash, H. Shokuhmand, Experimental and numerical investigation of the heat transfer augmentation and pressure drop in simple, dimpled and perforated dimpled louver fin banks with an in-line or staggered arrangement, Appl. Therm. Eng. 82 (2015) 194–205.
[24] J.Y. Jang, C.C. Chen, Optimization of louvered-fin heat exchanger with variable louver angles, Appl. Therm. Eng. 91 (2015) 138–150.
[25] Y.Y. Liang, C.C. Liu, C.Z. Li, J.P. Chen, Experimental and simulation study on the air side thermal hydraulic performance of automotive heat exchangers, Appl. Therm. Eng. 87 (2015) 305–315.
[26] A. Okbaz, A. Pınarbaşı, A.B. Olcay, 3D Computational Analysis of Thermal and Hydraulic Performance of Louvered Fin Heat Exchanger With Variable Louver Angle and Louver Pitch, 6B: Energy, 2016, V06BT08A025.
[27] A. Okbaz, A. Bahadır Olcay, M.S. Cellek, A. Pınarbaşı, Computational investigation of heat transfer and pressure drop in a typical louver fin-and-tube heat exchanger for various louver angles and fin pitches, in: EPJ Web Conf., 2084, 2017.
[28] A. Okbaz, Hüseyin Onbaşıoğlu, A. Bahadır Olcay and A. Pınarbaşı, "Investigation of Louvered Fin Heat Exchangers Performance via Experimental and Computational Fluid Dynamics Approach," Engineer and Machinery, 58, 687, 41–55, 2017.
[29] C.-C. Wang, C.-J. Lee, C.-T. Chang, S.-P. Lin, Heat transfer and friction correlation for compact louvered fin-and-tube heat exchangers, Int. J. Heat Mass Transf. 42 (11) (1999) 1945–1956.
[30] J. Dong, J. Chen, Z. Chen, W. Zhang, Y. Zhou, Heat transfer and pressure drop correlations for the multi-louvered fin compact heat exchangers, Energy Convers. Manage. 48 (5) (2007) 1506–1515.
[31] K. Ryu, K.S. Lee, Generalized heat-transfer and fluid-flow correlations for corrugated louvered fins, Int. J. Heat Mass Transf. 83 (2015) 604–612.
[32] ANSYS Fluent Theory Guide, 15317, November, 2013, pp. 724–746.

[33] C. Wang, K. Chi, Y. Chang, An experimental study of heat transfer and friction characteristics of typical louver fin-and-tube heat exchangers, Int. J. Heat Mass Transf. 41 (1998) 817–822.
[34] C. Wang, Y. Chang, Sensible heat and friction characteristics of plate fin-and-tube heat exchangers having plane fins,19, 4, 1996, pp. 223–230.
[35] W. Siddique, L. El-Gabry, I.V. Shevchuk, N.B. Hushmandi, T.H. Fransson, Flow structure, heat transfer and pressure drop in varying aspect ratio two-pass rectangular smooth channels, Heat Mass Transfer 48 (5) (2012) 735–748.
[36] I.V. Shevchuk, S.C. Jenkins, B. Weigand, J. von Wolfersdorf, S.O. Neumann, M. Schnieder, Validation and analysis of numerical results for a varying aspect ratio two-pass internal cooling channel, ASME J. Heat Transfer, 133, 5, 051701-1-051701-8, 2011
[37] A. Okbaz, A. olcay, A.B. Pinarbasi, Numerical investigation of fin rows number effects on thermal and hydraulic characteristics of louvered fin heat exchangers for experimental designs, Exp. Fluid Mech. 2014 (2014) 393–399.
[38] C.-C.C. Wang, C.-J. Lee, C.-T. Chang, S.-P. Lin, Heat transfer and friction correlation for compact louvered fm-and-tube heat exchangers, Int. J. Heat Mass Transf. 42 (11) (1999) 1945–1956.
[39] B. Sahin, N.A. Ozturk, C. Gurlek, Horseshoe vortex studies in the passage of a model plate-fin-and-tube heat exchanger, Int. J. Heat Fluid Flow 29 (1) (2008) 340–351.